

# Neutral-Neutral Synthesis of Organic Molecules in Cometary Comae

M. A. Cordiner,<sup>1,2\*</sup> and S. B. Charnley<sup>1</sup>

<sup>1</sup>*Astrochemistry Laboratory, NASA Goddard Space Flight Center, 8800 Greenbelt Road, Greenbelt, MD 20771, USA.*

<sup>2</sup>*Department of Physics, Catholic University of America, Washington, DC 20064, USA.*

Accepted for publication in MNRAS on April 16th 2021

## ABSTRACT

Remote and in-situ observations of cometary gases have revealed the presence of a wealth of complex organic molecules, including carbon chains, alcohols, imines and the amino acid glycine. Such chemical complexity in cometary material implies that impacts by comets could have supplied reagents for prebiotic chemistry to young planetary surfaces. However, the assumption that some of the molecules observed in cometary comae at millimetre wavelengths originate from ices stored inside the nucleus has not yet been proven. In fact, the comae of moderately-active comets reach sufficient densities within a few thousand kilometers of the nucleus for an active (solar radiation-driven) photochemistry to ensue. Here we present results from our latest chemical-hydrodynamic models incorporating an updated reaction network, and show that the commonly-observed HC<sub>3</sub>N (cyanoacetylene) and NH<sub>2</sub>CHO (formamide) molecules can be efficiently produced in cometary comae as a result of two-body, neutral-neutral, gas-phase reactions involving well-known coma gases. In the presence of a near-nucleus distributed source of CN (similar to that observed by the Rosetta spacecraft at comet 67P), we find that sufficient HC<sub>3</sub>N and NH<sub>2</sub>CHO can be synthesized to match the abundances of these molecules in previous observations of Oort Cloud comets. The precise origin of these (and other) complex organic molecules in cometary comae can be verified through interferometric mapping observations, for example, using the Atacama Large Millimeter/submillimeter Array (ALMA).

**Key words:** Comets: general – Astrochemistry – Methods: numerical

## 1 INTRODUCTION

Cometary ices are some of the most pristine, ancient materials in our Solar System. They have remained largely unaltered since they accreted during the birth of the planets (or earlier, in the interstellar medium), so their study provides unique information on the chemical conditions prevalent during the earliest history of our Solar System (Mumma & Charnley 2011; Altwegg et al. 2017). Comets are also believed to have delivered volatiles and organics during impacts with planets, so understanding their compositions provides insight into the chemical reagents that may have been present to drive prebiotic chemistry on the surfaces of Solar System bodies (Ehrenfreund & Charnley 2000; Martins & Sephton 2010).

Cometary ice abundances are derived primarily through multi-wavelength remote observations of their atmospheres/comae (Cochran et al. 2015), while in-situ spacecraft missions provide further details on select comets (*e.g.* Wyckoff et al. 1988; Rubin et al. 2019). Coma mapping observations reveal that several well-known cometary molecules (including C<sub>2</sub>, CN, HNC, H<sub>2</sub>CO and others) have “distributed” sources, identified through their extended, relatively flat spatial profiles (A’Hearn et al. 1995; Cottin & Fray 2008; Cordiner et al. 2014), compared with the strongly centrally-peaked spatial profiles of species released directly from the nucleus. Interpreted within the Haser (1957) paradigm of an isotropically-expanding, constant-velocity outflow, it is clear that

some ubiquitously-observed cometary molecules do not originate primarily from the nucleus, but instead arise in the coma, at distances of thousands to tens-of-thousands of kilometers from the nucleus. Coma “daughter” species are believed to be produced from the breakdown of larger “parent” molecules (sublimated directly from the nucleus), as a result of photodissociation. A plausible source for some of the observed distributed coma molecules is from the destruction of dust grains or large organic molecules in the coma (Cottin & Fray 2008). Recently, the amino acid glycine was detected by the Rosetta spacecraft during its mission to comet 67P Churyumov-Gerasimenko, with a radial density profile consistent with a distributed source, from the sublimation of ice-coated dust grains (Altwegg et al. 2016; Hadraoui et al. 2019).

Millimetre-wave spectroscopy has emerged as the leading ground-based method for identifying new coma molecules (*e.g.* Bockelée-Morvan et al. 2000; Biver et al. 2014), including the first detections of cyanoacetylene (HC<sub>3</sub>N), formamide (NH<sub>2</sub>CHO), formic acid (HCOOH), ethylene glycol (C<sub>2</sub>H<sub>6</sub>O<sub>2</sub>), and most recently: glycolaldehyde (C<sub>2</sub>H<sub>4</sub>O<sub>2</sub>) and ethanol (C<sub>2</sub>H<sub>5</sub>OH) (Biver et al. 2015). It is commonly assumed that they originate from the sublimation of ices stored inside the nucleus, but the presence of these species inside cometary nuclei is largely unproven. The majority of ground-based observations of organic molecules are made using single-pointing observations with a single-dish millimetre-wave telescope (such as the IRAM 30 m, with its ~ 10''-diameter angular resolution; corresponding to ~ 7000 km at 1 au Geocentric distance),

\* E-mail: martin.cordiner@nasa.gov

and are therefore lacking in spatial information required to constrain the nucleus vs. coma origins of these gases.

Rodgers & Charnley (2001a) used a chemical/hydrodynamic model (upon which our present study is based), to investigate the possible coma synthesis of four organic molecules (HCOOH, HCOOCH<sub>3</sub>, HC<sub>3</sub>N and CH<sub>3</sub>CN), which were detected in comet C/1995 O1 (Hale-Bopp) using radio spectroscopy. They determined that coma chemistry was insufficient to reproduce the observed abundances of these species. However, our latest models — which now include distributed sources of CN and H<sub>2</sub>CO in the coma — show that some molecules can, in fact, be produced rapidly as a result of gas-phase chemical reactions. Here we present chemical model calculations for HC<sub>3</sub>N and NH<sub>2</sub>CHO, demonstrating the synthesis of these species in detectable quantities.

## 2 MODEL

The details of our coma model were described by Rodgers & Charnley (2002), and the chemical network has been updated for carbon, nitrogen and oxygen-bearing species, as well as including negative ion chemistry (see Cordiner & Charnley 2014). The number densities ( $n_i$ ) of 283 gas-phase species ( $i$ ), and the temperatures ( $T_x$ ) of four fluids (neutrals, electrons and positive and negative ions) are calculated as a function distance ( $r$ ) from the nucleus, using the DVODE package (Hindmarsh 2019) to solve the following set of differential equations:

$$\frac{dn_i}{dr} = \frac{K_i}{v} - \frac{n_i}{v} \frac{dv}{dr} - \frac{2n_i}{r} \quad (1)$$

$$\frac{dT_x}{dr} = \frac{(\gamma_x - 1)T_x}{v} \left( \frac{G_x}{n_x k_B T_x} - \frac{2v}{r} - \frac{dv}{dr} - \frac{N_x}{(\gamma_x - 1)n_x} \right) \quad (2)$$

$$\frac{dv}{dr} = \frac{1}{\rho_s v^2 - (\gamma n k_B T)_s} \left( F_s v - ((\gamma - 1)G)_s - M_s v^2 + \frac{2v}{r} (\gamma n k_B T)_s \right) \quad (3)$$

The chemical source terms ( $K_i$ ) are equal to the sum over all production and loss rates for each species,  $v$  is the coma outflow velocity,  $T_x$  and  $N_x$  are the respective temperature and density source terms for each fluid ( $x$ ), and  $\gamma_x$  are the ratios of specific heat (Laplace's coefficient) of the fluids.  $G_x$  are the thermal energy source terms, which include contributions due to the chemical reaction enthalpies, collisions between ions, neutrals and electrons, radiative energy loss from H<sub>2</sub>O, and loss of fast H and H<sub>2</sub> from the coma.  $M$  and  $F$  are the mass and momentum source terms, respectively, and  $\rho$  is the mass density; subscript  $s$  implies summation over all four fluids in the model.

Parent gases are released from the nucleus and undergo isotropic expansion into the vacuum, reaching  $v = 0.7 \text{ km s}^{-1}$  by  $r = 1000 \text{ km}$ . The initial gas kinetic temperature was set to 100 K, with a nucleus radius of 2.5 km. The computed coma temperature and outflow velocity evolve in a very similar way to Figure 1 of Rodgers & Charnley (2002). Photodissociation of outflowing gases occurs due to solar radiation (using a nominal heliocentric distance  $R_h = 1 \text{ au}$ ), and the ensuing photochemistry is calculated following a network of 3842 reactions. Abundances of parent molecules are chosen for a typical ‘‘organic rich’’ comet (see Table 1); based on observations at infrared (Dello Russo et al. 2016) and radio (Bockelée-Morvan & Biver 2017) wavelengths, and supplemented by in-situ measurements of O<sub>2</sub> and N<sub>2</sub> in comet 67P by Bieler et al. (2015) and Rubin et al. (2019), respectively. We adopt an H<sub>2</sub>O production rate of

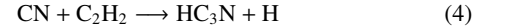
**Table 1.** Parent Abundances with Respect to H<sub>2</sub>O

Species	Abundance	Species	Abundance
H <sub>2</sub> O	1.00	CH <sub>4</sub>	0.01
CO <sub>2</sub>	0.10	NH <sub>3</sub>	0.01
CO	0.05	H <sub>2</sub> CO	$5.0 \times 10^{-3}$
O <sub>2</sub>	0.04	C <sub>2</sub> H <sub>2</sub>	$3.0 \times 10^{-3}$
CH <sub>3</sub> OH	0.04	HCN	$2.0 \times 10^{-3}$
C <sub>2</sub> H <sub>6</sub>	0.01	N <sub>2</sub>	$9.0 \times 10^{-4}$

$5 \times 10^{29} \text{ s}^{-1}$  (released directly from the nucleus), which is representative of a moderately active comet at  $R_h = 1 \text{ au}$ .

Our model has the ability to include distributed sources of molecules from the photolysis of (unidentified) parent species. In particular, we include distributed sources of H<sub>2</sub>CO and CN (named  $P1$  and  $P2$ , respectively), with photolysis rates of  $\Gamma_{P1} = 1.3 \times 10^{-4} \text{ s}^{-1}$  and  $\Gamma_{P2} = 3.23 \times 10^{-5} \text{ s}^{-1}$ . These rates were chosen to be consistent with previous observations showing spatially-extended distributions for these gases, with Haser parent scale lengths (at  $R_h = 1 \text{ au}$ ) of  $L_p = 5000 \text{ km}$  for H<sub>2</sub>CO (Biver et al. 2021) and  $L_p = 3.1 \times 10^4 \text{ km}$  for CN (Fray et al. 2005). An additional, inner-coma CN source ( $P3$ ) is also included in some of our models (see Section 3.1), based on a recent analysis of CN data from comet 67P (Hänni et al. 2020).

The synthesis of cyanoacetylene (HC<sub>3</sub>N) occurs in the coma *via* the following neutral-neutral, gas-phase reaction, measured in the laboratory by Lichtin & Lin (1986) and Sims et al. (1993):



Formamide (NH<sub>2</sub>CHO) is produced by the neutral-neutral reaction:



This reaction was studied theoretically by Barone et al. 2015 and Skouteris et al. 2017, who calculated it to be efficient at the low (10–100 K) temperatures found in interstellar clouds and cometary comae; we adopt the lower estimate for the rate coefficient ( $k = 7.79 \times 10^{-15} (T/300)^{-2.56} e^{-4.9/T} \text{ cm}^3 \text{ s}^{-1}$ ), from the latter study.

## 3 RESULTS

### 3.1 HC<sub>3</sub>N and NH<sub>2</sub>CHO

Figure 1 shows the number densities ( $n_i(r)$ ) of the molecules most relevant to this study, including parent species, photochemical daughters and products of coma chemistry. Three modeling scenarios are shown — Model A (panels (a) and (b)) includes a distributed source of H<sub>2</sub>CO from the breakdown of a large (unidentified) organic precursor molecule  $P1$  at distances  $r \sim 5000 \text{ km}$  from the nucleus (see Section 2), as well as two distributed sources of CN ( $P2$  and  $P3$ ), which give rise to peak gas-phase CN production at distances around  $r \sim 10^4 \text{ km}$  and  $r \sim 100 \text{ km}$ , respectively. Model B (panels (c) and (d)) has a single distributed source of H<sub>2</sub>CO ( $P1$ ) and a single, outer-coma distributed source of CN ( $P2$ ). Model C (panels (e) and (f)) has no additional distributed sources of H<sub>2</sub>CO or CN. In model C, H<sub>2</sub>CO is a parent species (Table 1) with a relatively short photolysis scale-length of  $\sim 10^4 \text{ km}$  (due to its large photolysis rate

$\Gamma_{\text{H}_2\text{CO}} = 2.3 \times 10^{-4} \text{ s}^{-1}$ ); however, there is still a significant contribution to the coma  $\text{H}_2\text{CO}$  abundance at distances  $r \sim 10^5 \text{ km}$  due to the photodissociation of methanol ( $\text{CH}_3\text{OH} + h\nu \rightarrow \text{H}_2\text{CO} + \text{H}_2$ ), which occurs at a slower rate (Huebner & Mukherjee 2015).

A significant source of the CN radical in all models is *via* the photodissociation reaction  $\text{HCN} + h\nu \rightarrow \text{CN} + \text{H}$ . Indeed, this is the dominant source of CN in Model C, but it was shown by Bockelée-Morvan & Crovisier (1985), A’Hearn et al. (1995), Fray et al. (2005) and Dello Russo et al. (2016) that the observed abundances of CN in comets are often inconsistent with a dominant origin from HCN photolysis. Furthermore, Fray et al. (2005) showed that the mean production scale length of CN in comets at  $R_h < 3 \text{ au}$  is not consistent with HCN photolysis, so an additional coma source of CN is indicated. Models A and B are therefore considered to better represent the chemistry of real comets. Using an initial abundance for the CN parent (P2) of 0.32 % with respect to  $\text{H}_2\text{O}$  (A’Hearn et al. 1995), Model B reaches a peak CN density of  $n_{\text{CN}} = 4.7 \times 10^3 \text{ cm}^{-3}$  around 800 km from the nucleus, whereas Model C (with no additional CN parent) reaches only  $n_{\text{CN}} = 1.0 \times 10^3 \text{ cm}^{-3}$ . The elevated CN density translates almost linearly to a larger  $\text{HC}_3\text{N}$  abundance *via* Equation (4). The distributed  $\text{H}_2\text{CO}$  source (from the breakdown of parent species P1) has a less noticeable impact on the overall coma  $\text{H}_2\text{CO}$  number density, which reaches  $n_{\text{H}_2\text{CO}} = 1.3 \times 10^3 \text{ cm}^{-3}$  at  $r = 10^4 \text{ km}$  in Model B and  $n_{\text{H}_2\text{CO}} = 0.8 \times 10^3 \text{ cm}^{-3}$  in Model C.

The total yield of  $\text{HC}_3\text{N}$  and  $\text{NH}_2\text{CHO}$  in our models is quantified using an “effective production rate”  $Q_e$ . This quantity is closely related to the observationally-derived production rate ( $Q$ ), and is defined as the production rate that would be measured from our model using a telescope beam diameter of 10” (the beam size of the IRAM 30-m telescope at 250 GHz), at a cometocentric distance of  $\Delta = 1 \text{ au}$ , under the assumption that the molecule of interest originates from the nucleus. The latter assumption has been employed in all previously published  $\text{HC}_3\text{N}$  and  $\text{NH}_2\text{CHO}$  production rates derived from ground-based mm-wave observations, so  $Q_e$  values allow our model output to be compared directly with observations taken at a similar cometocentric distance ( $\Delta \sim 1 \text{ au}$ ). The  $Q_e$  values (Table 2) are calculated by comparing our modeled column densities (averaged over a 10” beam) with a Haser parent model, using an outflow velocity equal to the column density-weighted mean HCN outflow velocity from our model ( $\langle v \rangle = 0.74 \text{ km s}^{-1}$ ), and photolysis rates from Huebner & Mukherjee (2015) and Heays et al. (2017). The HCN molecule is used for this purpose since HCN is a common probe of the coma outflow velocity at mm/sub-mm wavelengths, but use of other parent molecules such as  $\text{CH}_3\text{OH}$  and  $\text{H}_2\text{O}$  to measure  $\langle v \rangle$  produces very similar results. The  $Q_e$  values are then converted to effective abundances ( $a_e$ ) by taking the ratio with respect to the model  $\text{H}_2\text{O}$  production rate of  $5 \times 10^{29} \text{ s}^{-1}$ .

Upon inclusion of a distributed source of CN (P2), the effective  $\text{HC}_3\text{N}$  production rate increases by a factor of 5 from  $1.5 \times 10^{24} \text{ s}^{-1}$  to  $6.7 \times 10^{24} \text{ s}^{-1}$ , whereas a distributed  $\text{H}_2\text{CO}$  source (P1) only results in a modest, 4% increase to the  $\text{NH}_2\text{CHO}$  production rate. The corresponding effective abundances for model B (see Table 2) of  $1.4 \times 10^{-3} \%$  for  $\text{HC}_3\text{N}$  and  $1.0 \times 10^{-3} \%$  for  $\text{NH}_2\text{CHO}$  are significant — indeed, potentially detectable — but are still less than the lowest values reported in the literature for these molecules in Oort Cloud comets ( $2 \times 10^{-3} \%$  and  $8 \times 10^{-3} \%$ , respectively; Bockelée-Morvan & Biver 2017). Oort Cloud comets (OCCs) have relatively long orbital periods, covering distances up to hundreds of thousands of astronomical units from the Sun. They are observationally distinct from the Jupiter Family Comets (JFCs), which orbit at distances  $R_h \lesssim 10 \text{ au}$  and are exposed to more frequent, repeated heating during successive perihelion passages. Statistical studies show that

JFCs tend to be depleted relative to OCCs in some volatiles such as  $\text{CH}_4$ ,  $\text{C}_2\text{H}_2$  and  $\text{CO}$  (Dello Russo et al. 2016), and before the Rosetta mission to JFC 67P, there were no reported detections of  $\text{HC}_3\text{N}$  or  $\text{NH}_2\text{CHO}$  in any JFC. Both these molecules were detected early in the Rosetta mission by Le Roy et al. (2015) around  $R_h = 3.1 \text{ au}$ , but a more useful comparison is with the values measured by Rubin et al. (2019) closer to perihelion ( $R_h \sim 1.5 \text{ au}$ ) when the comet was more fully activated; these latter observations obtained  $\text{HC}_3\text{N}/\text{H}_2\text{O} = 4 \times 10^{-4} \%$  and  $\text{NH}_2\text{CHO}/\text{H}_2\text{O} = 4 \times 10^{-3} \%$ , respectively. Direct comparison between our model results and the measurements of comet 67P, however, requires the impact of the lower  $\text{H}_2\text{O}$  production rate of this comet to be considered (see Section 4).

A more prominent increase is seen in our model for both  $\text{HC}_3\text{N}$  and  $\text{NH}_2\text{CHO}$  when including a second distributed source of CN in the inner coma (P3). The properties of this additional source were chosen to match in-situ measurements of comet 67P (Churyumov-Gerasimenko) by the Rosetta spacecraft (Hänni et al. 2020). Throughout the mission to 67P, the ROSINA mass spectrometer detected a clear signal due to gas-phase CN at cometocentric distances 20–200 km, with a local abundance ratio of  $\sim 0.01$ – $0.1$  with respect to HCN at dates around perihelion. The CN spatial distribution was observed to be relatively flat compared with  $\text{H}_2\text{O}$  and other parent species in the coma, consistent with a distributed source of CN, with an abundance far in excess of what could be explained by photolysis of any known coma nitriles (see also Hänni et al. 2021). The observed excess CN signal was tentatively attributed by Hänni et al. (2020) to the breakdown of CN-bearing refractory particles, such as salts (ammonium cyanide —  $\text{NH}_4\text{CN}$ , for example), nitrogen-rich dust, or organic macromolecules. The production rate ( $Q_{\text{P3}}/Q_{\text{H}_2\text{O}} = 6 \times 10^{-3}$ ) and photolysis rate ( $\Gamma_{\text{P3}} = 3.5 \times 10^{-2} \text{ s}^{-1}$ ) of this additional (unidentified) CN parent were chosen in our model to produce a maximum  $n_{\text{CN}}/n_{\text{HCN}}$  ratio of  $\approx 0.05$  between  $r = 100$ – $200 \text{ km}$  from the nucleus, in line with the ROSINA measurements close to perihelion.

As a consequence of the increased CN density in the inner coma, Equation (4) proceeds more rapidly and the  $\text{HC}_3\text{N}$  effective abundance in Model A increases to 0.018%. The presence of additional CN has several other knock-on effects for the coma chemistry. In particular, the CN radical quickly reacts with  $\text{NH}_3$  (sublimating from the nucleus) to produce  $\text{HCN} + \text{NH}_2$  (Sims et al. 1994; Talbi & Smith 2009). Some of this additional  $\text{NH}_2$  reacts with  $\text{H}_2\text{CO}$  (*via* Equation 5) to produce  $\text{NH}_2\text{CHO}$ , leading to a significant (factor of 12) increase in the  $\text{NH}_2\text{CHO}$  abundance, which then reaches  $a_e = 0.012\%$ . Consequently, in Model A, both  $\text{HC}_3\text{N}$  and  $\text{NH}_2\text{CHO}$  attain abundances with respect to  $\text{H}_2\text{O}$  that are well within the range of values previously detected in Oort Cloud comets (0.002–0.068% for  $\text{HC}_3\text{N}$  and 0.008–0.021% for  $\text{NH}_2\text{CHO}$ ; Bockelée-Morvan & Biver 2017), with no need for a nucleus (parent) source of either molecule.

### 3.2 Other Molecules

The reaction between CN and  $\text{O}_2$  was studied in the laboratory by Sims et al. (1994), and found to proceed rapidly at low temperatures. Feng & Hershberger 2009 determined  $\text{OCN} + \text{O}$  to be the dominant product channel, so large amounts of OCN are produced in our models. The effective OCN abundance inside a 10” beam is  $a_e = 0.2\%$  in Model A and  $a_e = 4 \times 10^{-3} \%$  in Model B, assuming a generic photolysis rate of  $\Gamma_{\text{OCS}} = 10^{-5} \text{ s}^{-1}$ . Gas-phase OCN was detected by the Rosetta spacecraft in the coma of comet 67P during a dust impact event (Altwegg et al. 2020), but has not yet been detected in any other comets. It has a moderate dipole moment of

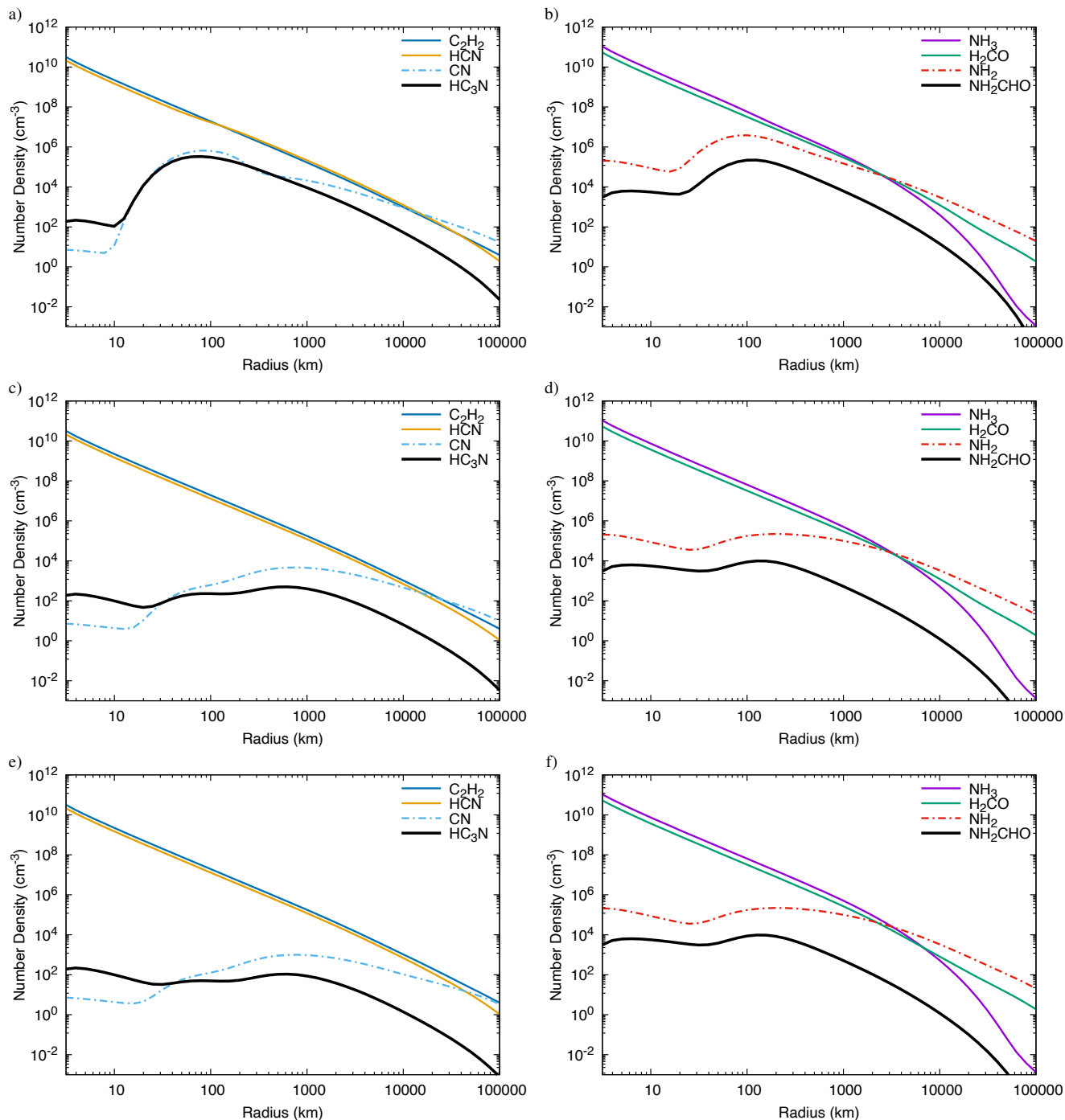


**Figure 1.** Coma model output showing molecular number densities as a function of radius. Parent species are shown with solid, colored curves, and photolysis products are shown with dot-dashed line styles. Thick black curves show HC<sub>3</sub>N (left column) and NH<sub>2</sub>CHO (right column), formed as a result of Equations (4) and (5), respectively. Results from Model A (panels (a) and (b); top row) include a distributed source of H<sub>2</sub>CO (*P1*) and two distributed sources of CN (*P2* and *P3*). Model B are (panels (c) and (d); middle row), and have single distributed sources of CN (*P2*) and H<sub>2</sub>CO (*P1*). Panels (e) and (f) (bottom row) are for Model C, which is the base model, with no additional sources of CN or H<sub>2</sub>CO.

0.64 D, with several rotational transitions in the millimetre and sub-millimetre range. Consequently, if the coma CN and O<sub>2</sub> abundances are similar to those measured in comet 67P close to perihelion, OCN may be bright enough to be detectable in a sufficiently active Oort Cloud comet. Indeed, since CN + O<sub>2</sub> is the main pathway to OCN in our model (other pathways are negligible), a measurement of the OCN production rate could be used to infer the product of CN × O<sub>2</sub>

abundances in the inner coma of future comets, thus providing an indirect measurement of the O<sub>2</sub> abundance, which has so far been impossible to obtain with ground-based observations.

A smaller, but still significant, amount of NO is also produced as a result of the alternative product channel CN + O<sub>2</sub> → CO + NO. The resulting NO goes on to react with OCN to produce N<sub>2</sub>O and CO.

**Table 2.** Effective Production Rates ( $Q_e$ ) and Abundances ( $a_e = Q_e/Q_{\text{H}_2\text{O}}$ ) from our Coma Models

Species	Model A		Model B		Model C	
	$Q_e$ ( $10^{24} \text{ s}^{-1}$ )	$a_e$ (%)	$Q_e$ ( $10^{24} \text{ s}^{-1}$ )	$a_e$ (%)	$Q_e$ ( $10^{24} \text{ s}^{-1}$ )	$a_e$ (%)
HC <sub>3</sub> N	87.3	$1.8 \times 10^{-2}$	6.7	$1.4 \times 10^{-3}$	1.5	$2.9 \times 10^{-4}$
NH <sub>2</sub> CHO	58.1	$1.2 \times 10^{-2}$	4.9	$1.0 \times 10^{-3}$	4.7	$9.4 \times 10^{-4}$

In addition to the main product channel (leading to  $\text{NH}_2 + \text{HCN}$ ), the reaction between  $\text{CN} + \text{NH}_3$  was suggested by [Herbst et al. \(1994\)](#) as a possible source of  $\text{NH}_2\text{CN}$  (cyanamide) in the interstellar medium. If this reaction proceeds with reasonable efficiency,  $\text{NH}_2\text{CN}$  could reach detectable abundances in the inner coma (0.08% in Model A, assuming an  $\text{NH}_2\text{CN}$  product branching ratio of 1/3). More recent quantum calculations by [Talbi & Smith \(2009\)](#), however, indicate that this product channel may be negligible in comparison to the  $\text{NH}_2 + \text{HCN}$  channel.

### 3.3 Synthetic Coma Maps

Our predictions regarding the origins of cometary HC<sub>3</sub>N and NH<sub>2</sub>CHO (and other molecules) in comets, may be tested through mapping observations of their spatial distributions with respect to the nucleus. Parent molecules (released directly from the nucleus) have compact brightness distributions that fall rapidly as  $\sim 1/\rho$ , where  $\rho$  is the nucleocentric distance projected in the plane of the sky. Daughter species (or products of coma chemistry), on the other hand, have flatter, more extended distributions. These two scenarios can be readily distinguished through interferometric millimetre/submillimetre observations (for example, using the ALMA telescope; [Cordiner et al. 2014](#)), or using a single-dish facility, in the case of an unusually close-up apparition (such as 252P/Linear in 2016, which reached a Geocentric distance of only 0.04 au; [Coulson et al. 2017](#)). Detailed coma mapping observations can also provide crucial information on production scale-lengths for comparison with numerical models, to help elucidate the specific production pathway for the species in question.

Synthetic mm-wave flux maps are shown for the case of HC<sub>3</sub>N as a parent molecule in Figure 2 (top panel), and for HC<sub>3</sub>N produced from the reaction of CN with C<sub>2</sub>H<sub>2</sub> according to Model B (bottom panel). These maps were constructed for the  $J = 26 - 25$  transition by raytracing the 3D projection of our model density output along the observer-comet sightline, using the RATRAN Sky code ([Hogerheijde & van der Tak 2000](#)). An excitation temperature of 50 K and Geocentric distance  $\Delta = 1$  au were assumed, and the resulting maps were integrated along the spectral axis, then convolved with a Gaussian beam of FWHM = 1'', similar to ALMA's lowest resolution at this frequency. Distributed sources with parent scale lengths less than a few thousand kilometers are difficult to map reliably using a single-dish facility such as the IRAM 30 m telescope, as shown by the extent of the scale bars relative to the synthetic brightness distributions in Figure 2. ALMA observations, on the other hand, are readily able to distinguish between the two scenarios, and can therefore provide proof of a nucleus or coma origin for HC<sub>3</sub>N, NH<sub>2</sub>CHO and other species.

Previous analyses of observational data obtained using radio interferometry of cometary gases have relied on simple Haser models to interpret the observed spatial profiles for distributed coma species such as H<sub>2</sub>CO, HNC and CS ([Boissier et al. 2007](#); [Cordiner et al.](#)

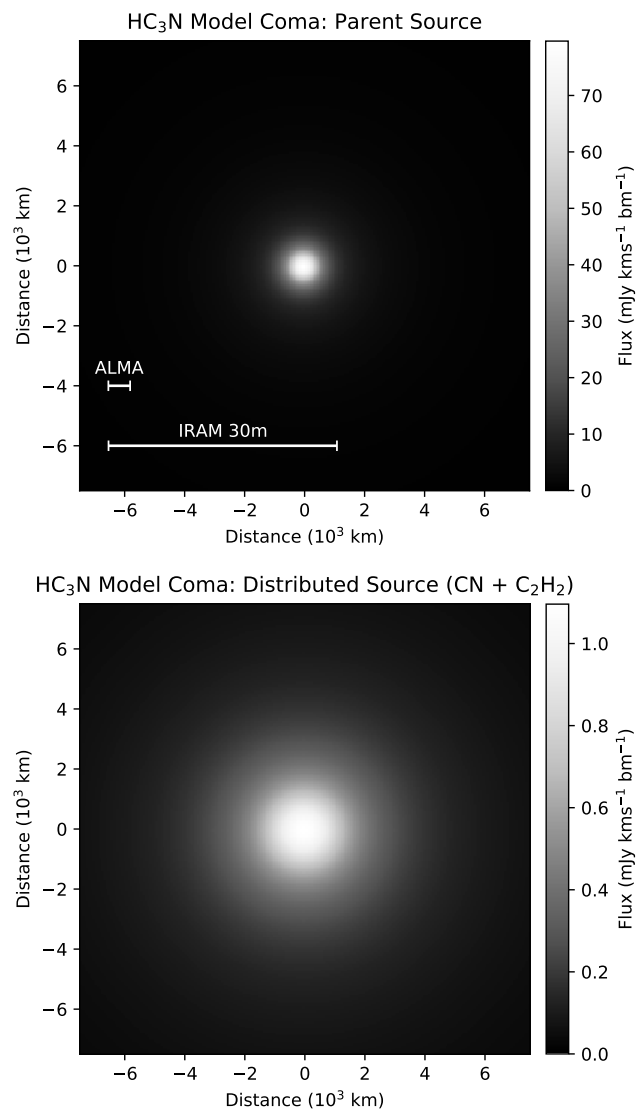


**Figure 2.** Simulated HC<sub>3</sub>N coma images (flux maps) for the  $J = 26 - 25$  transition at 236.5 GHz, assuming an excitation temperature of 50 K, smoothed to an angular resolution (beam FWHM) of 1''. The top panel is for HC<sub>3</sub>N as a parent (sublimating directly from the nucleus with  $Q(\text{HC}_3\text{N}) = 10^{26} \text{ s}^{-1}$ ). Bottom panel is for HC<sub>3</sub>N produced *via* Equation (4), according to the model density profile in Figure 1 (panel c). Horizontal scale bars in the top panel indicate the characteristic spatial resolution of the ALMA and IRAM 30-m telescopes (1'' and 10'', respectively).

2014, 2017). This approach assumes the detected molecules arise only as a result of photodissociation of a single parent species, and that the parent species (as well as the daughter species in question) does not have any additional sources or sinks as a result of chemical reactions or dust sources in the coma. Coma chemistry results in radial density profiles that can be distinctly different from Haser-model density profiles (see Figure 1), so sufficiently detailed (high signal-to-noise) ALMA observations should have the ability to distinguish between different chemical production scenarios, as well as photodissociation, production from icy grains, and sublimation from the nucleus (or a combination these mechanisms).

#### 4 DISCUSSION

Our chemical models show that significant quantities of  $\text{HC}_3\text{N}$ ,  $\text{NH}_2\text{CHO}$  and other molecules can be synthesized in the coma through neutral-neutral reactions involving simple chemical precursor species ( $\text{CN}$ ,  $\text{C}_2\text{H}_2$ ,  $\text{NH}_2$ ,  $\text{O}_2$  and  $\text{H}_2\text{CO}$ ), already known to be abundant from previous comet observations. The presence of a distributed source of  $\text{CN}$  in the inner coma (as observed by Hänni et al. 2020 for comet 67P), strongly enhances the efficiency of both reactions (4) and (5), bringing the effective abundances for Model A (see Table 2) into the range of previously observed values for these molecules. The presence of such an additional  $\text{CN}$  source is consistent not only with Rosetta measurements of comet 67P, but also with previous studies regarding the (still unidentified) source of the closely-related  $\text{HNC}$  molecule in comets (see Cordiner et al. 2017, and references therein).

When  $\text{HNC}$  was first detected in comet C/1995 O1 (Hale-Bopp), the large  $\text{HNC}/\text{HCN}$  mixing ratio (similar to the value found in the interstellar medium) was taken as evidence that pristine (unprocessed) interstellar material may be incorporated into cometary nuclei. However, maps of the  $\text{HNC}$  spatial distribution in comet Hale-Bopp (Blake et al. 1999), as well as strong variability of the  $\text{HNC}/\text{HCN}$  ratio with heliocentric distance in a sample of 14 comets (Lis et al. 2008), pointed towards a distributed (coma) source of  $\text{HNC}$ , which was hypothesized to originate from the breakdown of macromolecular or dust precursor material (see also Rodgers & Charnley 2001b). Detailed interferometric mapping using the Atacama Large Millimeter/submillimeter Array (ALMA) provided definitive evidence for a distributed source of  $\text{HNC}$  at distances of a few hundred kilometers from the nucleus of comet C/2013 S1 (ISON), leading to the conclusion that this molecule most likely originates from the degradation of nitrogen-rich organic refractory material (Cordiner et al. 2014, 2017).

Low-mass, refractory organic particles (CHON grains) were detected in large abundances in comet 1P/Halley by the Giotto mission (Kissel et al. 1986), and Wyckoff et al. (1991) determined that 90% of this comet's nitrogen budget was contained within the refractory dust component. More recent in-situ work on comet 67P using the Rosetta COSIMA instrument revealed the presence of very large macromolecular compounds in the cometary dust, analogous to the insoluble organic matter present in carbonaceous meteorites (Fray et al. 2016). With a mean N/C ratio of 3.5% (Fray et al. 2017), this material presents a plausible source of additional  $\text{CN}$  radicals in the coma, among other small N-bearing organics. Macromolecules such as  $\text{HCN}$  polymer or hexamethylenetetramine (HMT, recently detected in meteorites by Oba et al. 2020) present another possible source of coma  $\text{CN}$ , but these specific compounds are yet to be found in cometary samples. Polyoxymethylene (POM, or formaldehyde polymer) has been studied extensively as another plausible macro-

molecular grain component in comets, and detailed models show that POM could explain the distributed  $\text{H}_2\text{CO}$  sources in comets 1P/Halley and C/1995 O1 (Hale-Bopp) (Cottin et al. 2004; Fray et al. 2006).

Hänni et al. (2020) also considered the dissociation of  $\text{NH}_4\text{CN}$  as a plausible source of  $\text{CN}$  in the inner coma of comet 67P. The  $\text{NH}_4\text{CN}$  salt (also known as  $\text{NH}_4^+\text{CN}^-$ ) is unstable in the gas phase, but could be carried into the coma as a solid embedded in (or adsorbed on the surface of) dust grains, before sublimating and dissociating. The possibility of ammoniated salts as a reservoir of  $\text{HCN}$  and  $\text{NH}_3$  in comets was first discussed by Mumma et al. (2018). Altwegg et al. (2020) reported the likely presence of five different ammonium salts ( $\text{NH}_4^+\text{X}^-$ , where  $\text{X}^-$  is a deprotonated acid, such as  $\text{Cl}^-$ ,  $\text{NCO}^-$  or  $\text{HCOO}^-$ ) in the coma of comet 67P, based on ROSINA mass spectrometry during a dust impact event. Evidence for abundant ammonium salts on 67P's surface (including  $\text{NH}_4\text{CN}$ ) was also found with Rosetta infrared spectroscopy (Poch et al. 2020).

While  $\text{HCN} + \text{NH}_3$  is believed to be the dominant dissociation channel of  $\text{NH}_4\text{CN}$ , other products are possible (Altwegg et al. 2020; Hänni et al. 2020). By analogy with the dissociation of  $\text{NH}_4\text{Cl}$ , which has been studied using ab-initio methods, as well as in the laboratory (see Hänni et al. 2019 and references therein), it is suggested that  $\text{CN}$  and  $\text{CN}^-$  could be products of  $\text{NH}_4\text{CN}$  dissociation. Our models show that the majority of  $\text{CN}^-$  produced in the inner coma from the spontaneous dissociation reaction  $\text{NH}_4\text{CN} \rightarrow \text{NH}_4^+ + \text{CN}^-$  would be converted almost immediately to neutral  $\text{CN}$  (+ H) upon collision with  $\text{NH}_4^+$  (see Harada & Herbst 2008). This therefore represents another possible source of  $\text{CN}$  to drive the neutral-neutral synthesis of  $\text{HC}_3\text{N}$  and  $\text{NH}_2\text{CHO}$ . More laboratory studies of  $\text{NH}_4\text{CN}$  dissociation products are needed to confirm this hypothesis.

In light of the recent detections of salts in comet 67P, the results of Hänni et al. (2019) and Altwegg et al. (2020) imply a possible contribution to the  $\text{NH}_2\text{CHO}$  coma abundance from  $\text{NH}_4\text{COOH}$  (ammonium formate) salt dissociation. Our models show that the presence of additional sources of molecules in the inner coma (such as  $\text{NH}_3$  and  $\text{HCN}$ ), from the dissociation of salts including ammonium formate, ammonium cyanide and ammonium cyanate (see Altwegg et al. 2020), lead to increased abundances of complex organics as a result of subsequent gas-phase reactions. Further investigations of the coma chemistry arising from such reactions are therefore warranted. The injection of ions, radicals and other reactive neutrals into the inner coma, following the dissociation of ammonium salts, would give rise to further, previously unstudied chemical processes in the outflowing cometary gas. To model this in detail, however, would require improved knowledge of the initial salt abundances and their full range of dissociation products, as well as the inclusion of a population of outflowing, sublimating grains into our model, which is beyond the scope of the present study.

Our findings for  $\text{HC}_3\text{N}$  are in contrast to Rodgers & Charnley (2001a), whose model predicted a low  $\text{HC}_3\text{N}/\text{H}_2\text{O}$  abundance ratio (averaged inside an 11'' beam) of  $7 \times 10^{-4} \%$  for Hale-Bopp, compared with the observed value of  $1.7 \times 10^{-2} \%$ . In their model,  $\text{HC}_3\text{N}$  formation was driven by the  $\text{CN} + \text{C}_2\text{H}_2$  reaction (4), with  $\text{CN}$  produced photolytically from  $\text{HCN}$  released directly from the nucleus. Consequently, they concluded that the observed  $\text{HC}_3\text{N}$  could not be synthesized in the coma by Equation (4) alone, and is therefore likely to be present in the nuclear ice. The Rodgers & Charnley (2001a) model should have been more efficient than ours at producing  $\text{HC}_3\text{N}$  due to the omission of the (experimentally observed) 20 K activation energy barrier in Equation (4), allowing the reaction to proceed more rapidly at low temperatures in their model. The ability of our new model to effectively reproduce the  $\text{HC}_3\text{N}$  observations is attributed

primarily to the inclusion of the two distributed sources of CN (*P2* and *P3*) in the coma for Model A, which were not considered by [Rodgers & Charnley \(2001a\)](#).

It is interesting to note that  $\text{HC}_3\text{N}/\text{H}_2\text{O}$  ratio in comet 67P ( $4 \times 10^{-4}$ ; [Rubin et al. 2019](#)) is significantly lower than in the sample of Oort Cloud comets observed to-date ( $2 \times 10^{-3}$ – $6.8 \times 10^{-4}$ ; [Bockelée-Morvan & Biver 2017](#)). Our modeling work provides a natural explanation for this, without requiring peculiar/anomalously-low  $\text{HC}_3\text{N}$  abundances in 67P's nucleus compared with OCCs. To investigate the production of  $\text{HC}_3\text{N}$  (and  $\text{NH}_2\text{CHO}$ ) in lower-density coma environments such as that of 67P, we ran additional model calculations spanning a range of water production rates  $Q_{\text{H}_2\text{O}} = 3 \times 10^{27}$ – $5 \times 10^{30} \text{ s}^{-1}$  (covering the range of values observed in typical cometary apparitions). The chemical reaction rates for formation and destruction of the species of interest in our study vary as nonlinear functions of the coma density and temperature, so the changes in their coma abundances in response to  $Q_{\text{H}_2\text{O}}$  is nontrivial. The results of our tests show that for  $Q_{\text{H}_2\text{O}}$  above a few times  $10^{29} \text{ s}^{-1}$ , the  $\text{HC}_3\text{N}$  and  $\text{NH}_2\text{CHO}$  abundances with respect to water are not strongly dependent on the production rate (they vary by  $< 15\%$  in this  $Q_{\text{H}_2\text{O}}$  range). For  $Q_{\text{H}_2\text{O}} \lesssim 10^{29} \text{ s}^{-1}$ , the size of the region dense enough for rapid neutral-neutral reactions to occur shrinks considerably, leading to significant reductions in the yields of  $\text{HC}_3\text{N}$  and  $\text{NH}_2\text{CHO}$  via reactions (4) and (5).

To simulate comet 67P for comparison with Rosetta mass spectrometry measurements, we ran the  $Q_{\text{H}_2\text{O}} = 3 \times 10^{27} \text{ s}^{-1}$  model at  $R_h = 1.5 \text{ au}$ , using [Rubin et al. \(2019\)](#)'s measured parent abundances and observational circumstances ( $\text{C}_2\text{H}_2$  was not measured by [Rubin et al. 2019](#), so we adopt the mean JFC mixing ratio of 0.07% for this species, from [Dello Russo et al. 2016](#)). The inner-coma CN production rate was scaled to reproduce the CN/HCN ratio measured by [Hänni et al. \(2020\)](#) around the time of the [Rubin et al. \(2019\)](#) measurements, and our modeled abundances ( $a(X)$ , with respect to  $\text{H}_2\text{O}$ ) were extracted at a distance of 220 km from the nucleus, which is close to the average distance at which the [Rubin et al. \(2019\)](#) measurements were obtained. For Model A, we find  $a(\text{HC}_3\text{N}) = 3.0 \times 10^{-4} \%$  and  $a(\text{NH}_2\text{CHO}) = 1.5 \times 10^{-5} \%$ ; for model B:  $a(\text{HC}_3\text{N}) = 5.5 \times 10^{-6} \%$  and  $a(\text{NH}_2\text{CHO}) = 1.1 \times 10^{-5} \%$ ; and for model C:  $a(\text{HC}_3\text{N}) = 8.9 \times 10^{-7} \%$  and  $a(\text{NH}_2\text{CHO}) = 1.1 \times 10^{-5} \%$ . These values can be compared with the Rosetta measurements of  $a(\text{HC}_3\text{N}) = (4 \pm 2) \times 10^{-4} \%$  and  $a(\text{NH}_2\text{CHO}) = (4 \pm 2) \times 10^{-3} \%$ . The agreement for  $\text{HC}_3\text{N}$  (within the observational uncertainties) using Model A is surprisingly good considering the uncertain radial density profile of the inner-coma CN source. Our  $\text{HC}_3\text{N}/\text{HCN}$  ratio of  $2.1 \times 10^{-3}$  is also in agreement with the value of  $(2.9 \pm 1.9) \times 10^{-3}$  from [Rubin et al. \(2019\)](#), but is somewhat less than the mean value of  $(4.6 \pm 0.8) \times 10^{-3}$  measured by [Hänni et al. \(2021\)](#) between  $R_h = 1.24$ – $1.74 \text{ au}$ . This discrepancy could be accounted for by variability in the CN, HCN and  $\text{C}_2\text{H}_2$  abundances during the extended (5 month) time period covered by the [Hänni et al. \(2021\)](#) study. We note, however, that purely gas-phase chemistry would be expected to give rise to a steeper slope in the  $\text{HC}_3\text{N}/\text{HCN}$  ratio as a function of heliocentric distance than observed in 67P, so some contribution from an additional (nucleus) source seems likely. For  $\text{NH}_2\text{CHO}$ , the failure of all our models to reproduce the measured abundance in comet 67P by more than two orders of magnitude implies the presence of an additional source for this molecule — for example, from the dissociation of  $\text{NH}_4\text{COOH}$  salt ([Hänni et al. 2019](#)), or from sublimation of  $\text{NH}_2\text{CHO}$  ice directly from the nucleus, albeit with a substantially lower abundance than found previously in Oort Cloud comets ([Bockelée-Morvan & Biver 2017](#)).

Our modeling work implies that  $\text{HC}_3\text{N}$  and  $\text{NH}_2\text{CHO}$  could be

present in cometary nuclei at abundances that are significantly less than implied by previous (ground-based) observations. There is some evidence that the abundances of  $\text{HC}_3\text{N}$  and  $\text{NH}_2\text{CHO}$  are enhanced in typical cometary comae compared with the warm envelope of the solar-type protostar IRAS 16293-2422, which is rich in the sublimated interstellar ices believed to be a major constituent of comets ([Kahane et al. 2013](#); [Jaber Al-Edhari et al. 2017](#); [Drozdovskaya et al. 2019](#)). On the other hand, the protostellar  $\text{HC}_3\text{N}/\text{HCN}$  ratio (which is easier to measure from the ground than the ratio with respect to  $\text{H}_2\text{O}$ ) is only marginally smaller in IRAS 16293-2422 (0.36%; [Drozdovskaya et al. 2019](#)) than in 67P (0.44%; [Hänni et al. 2021](#); full Rosetta mission). Gas-phase  $\text{HC}_3\text{N}/\text{HCN}$  ratios may be even larger in protoplanetary disks (3–134%, depending on the assumed temperature; [Bergner et al. 2018](#)), so it is likely that  $\text{HC}_3\text{N}$  can be incorporated into cometary nuclei during their accretion out of ice in the disk mid-plane. Comparison between cometary and interstellar/protostellar/disk abundances is nontrivial due to the possibility of chemical alteration during the passage of interstellar ices into the protoplanetary disk mid-plane and ultimately, into cometary nuclei. Indeed,  $\text{HC}_3\text{N}$  abundances are subject to significant modification by gas-phase processing in the warm regions surrounding the protostar ([Walsh et al. 2014](#)). Nevertheless, our results show that chemical processing in the coma can lead to elevated abundances of some organic molecules, and this possibility should be taken into account when comparing abundances between interstellar ices and cometary comae, as a means for obtaining insights into the origin of cometary matter.

Impacts between comets and planets were common during the early history of the Solar System, and may have allowed the delivery of organic molecules to planetary surfaces (e.g. [Pierazzo & Chyba 1999](#); [McCaffrey et al. 2014](#); [Todd & Öberg 2020](#)). Both  $\text{HC}_3\text{N}$  and  $\text{NH}_2\text{CHO}$  have been implicated in the prebiotic synthesis of amino acids and DNA nucleobases on the primordial Earth ([Ferris et al. 1968](#); [Saladino et al. 2012](#); [Patel et al. 2015](#)). Our finding that these molecules may be less abundant in cometary ices than previously believed could therefore be of importance for theories concerning the chemical inventory of material available for the origin of life.

An important caveat concerning the extent of  $\text{HC}_3\text{N}$  and  $\text{NH}_2\text{CHO}$  synthesis in comets as a result of gas-phase coma chemistry is the uncertainty regarding the additional distributed CN sources (*P2* and *P3*). The survey of [Dello Russo et al. \(2016\)](#) identified variability in the importance of the primary extended source of CN (*P2*) throughout the comet population, and the inner-coma CN source (*P3*) has only been detected in a single comet to-date (67P, although we are not aware of any dedicated attempts to detect a distinct, inner-coma CN source in any other comets). In our Model A, *P3* was introduced as a photochemical source of CN, with a production rate and scale length tailored to reproduce the CN/HCN ratio measured by [Hänni et al. \(2020\)](#) in comet 67P. However, the detailed radial behaviour of this CN source is not yet well constrained, and it remains to be determined how well the CN abundance in Oort Cloud comets may be represented by the CN/HCN ratio in 67P. Consequently, although we believe our models represent plausible scenarios for moderately-active OCCs, the specific, numerical results remain uncertain until inner-coma CN measurements are made in a larger sample of comets, and the properties of the dominant coma CN sources are fully elucidated.

## 5 CONCLUSION

Our chemical models for a moderately active comet, with organic-rich parent abundances, demonstrate that gas-phase synthesis of HC<sub>3</sub>N and NH<sub>2</sub>CHO occurs as a result of neutral-neutral reactions between simple precursor molecules known to be abundant in the coma. The presence of a distributed CN source in the inner coma, similar to that observed by Rosetta in comet 67P, increases the efficiency of these reactions, leading to effective HC<sub>3</sub>N and NH<sub>2</sub>CHO abundances in our model that can reach levels similar to those observed in moderately high-activity comets using ground-based millimetre-wave observations. Neutral-neutral coma chemistry can also reproduce the lower HC<sub>3</sub>N/H<sub>2</sub>O ratio measured by Rosetta in the relatively low-activity comet 67P before perihelion at  $R_h \sim 1.5$  au. As a result of such active gas-phase chemistry, the abundances of complex organics in the coma are therefore not necessarily representative of those stored in the nucleus ice. High-resolution mapping using millimetre/submillimetre facilities such as ALMA will be crucial for determining the importance of nucleus vs. coma sources for these, and other complex organic molecules in future cometary apparitions. Additional observations, laboratory work, and modeling will be required to elucidate the distribution and origin of the inner-coma CN sources in comets other than 67P, and to determine the full impact of the dissociation products from ammonium salts and organic macromolecules on coma chemistry.

## ACKNOWLEDGEMENTS

This research was supported by the NASA Planetary Science Division Internal Scientist Funding Program through the Fundamental Laboratory Research work package (FLaRe).

## REFERENCES

- A'Hearn M. F., Millis R. C., Schleicher D. O., Osip D. J., Birch P. V., 1995, *Icarus*, **118**, 223
- Altwegg K., et al., 2016, *Science Advances*, **2**, e1600285
- Altwegg K., et al., 2017, *Philosophical Transactions of the Royal Society of London Series A*, **375**, 20160253
- Altwegg K., et al., 2020, *Nature Astronomy*, **4**, 533
- Barone V., Latouche C., Skouteris D., Vazart F., Balucani N., Ceccarelli C., Lefloch B., 2015, *MNRAS*, **453**, L31
- Bergner J. B., Guzmán V. G., Öberg K. I., Loomis R. A., Pegues J., 2018, *ApJ*, **857**, 69
- Bieler A., et al., 2015, *Nature*, **526**, 678
- Biver N., et al., 2014, *A&A*, **566**, L5
- Biver N., et al., 2015, *Science Advances*, **1**, 1500863
- Biver N., et al., 2021, *A&A*, p. in press
- Blake G. A., Qi C., Hogerheijde M. R., Gurwell M. A., Muhleman D. O., 1999, *Nature*, **398**, 213
- Bockelée-Morvan D., Biver N., 2017, *Philosophical Transactions of the Royal Society of London Series A*, **375**, 20160252
- Bockelée-Morvan D., Crovisier J., 1985, *A&A*, **151**, 90
- Bockelée-Morvan D., et al., 2000, *A&A*, **353**, 1101
- Boissier J., Bockelée-Morvan D., Biver N., Crovisier J., Despois D., Marsden B. G., Moreno R., 2007, *A&A*, **475**, 1131
- Cochran A. L., et al., 2015, *Space-Sci.-Rev.*, **197**, 9
- Cordiner M. A., Charnley S. B., 2014, *Meteoritics and Planetary Science*, **49**, 21
- Cordiner M. A., et al., 2014, *ApJL*, **792**, L2
- Cordiner M. A., et al., 2017, *ApJ*, **838**, 147
- Cottin H., Fray N., 2008, *Space-Sci.-Rev.*, **138**, 179
- Cottin H., Bénilan Y., Gazeau M.-C., Raulin F., 2004, *Icarus*, **167**, 397
- Coulson I. M., et al., 2017, *AJ*, **153**, 169
- Dello Russo N., Kawakita H., Vervack R. J., Weaver H. A., 2016, *Icarus*, **278**, 301
- Drozdzovskaya M. N., van Dishoeck E. F., Rubin M., Jørgensen J. K., Altwegg K., 2019, *MNRAS*, **490**, 50
- Ehrenfreund P., Charnley S. B., 2000, *ARA&A*, **38**, 427
- Feng W., Hershberger J. F., 2009, *Journal of Physical Chemistry A*, **113**, 3523
- Ferris J. P., Sanchez R. A., Orgel L. E., 1968, *J. Mol. Bio.*, **33**, 693
- Fray N., Bénilan Y., Cottin H., Gazeau M. C., Crovisier J., 2005, *Planet. Space Sci.*, **53**, 1243
- Fray N., Bénilan Y., Biver N., Bockelée-Morvan D., Cottin H., Crovisier J., Gazeau M.-C., 2006, *Icarus*, **184**, 239
- Fray N., et al., 2016, *Nature*, **538**, 72
- Fray N., et al., 2017, *MNRAS*, **469**, S506
- Hadraoui K., et al., 2019, *A&A*, **630**, A32
- Hänni N., et al., 2019, *The Journal of Physical Chemistry A*, **123**, 5805
- Hänni N., Altwegg K., Pestoni B., Rubin M., Schroeder I., Schuhmann M., Wampfler S., 2020, *MNRAS*, **498**, 2239
- Hänni N., et al., 2021, *A&A*, **647**, A22
- Harada N., Herbst E., 2008, *ApJ*, **685**, 272
- Haser L., 1957, *Bulletin de la Societe Royale des Sciences de Liege*, **43**, 740
- Heays A. N., Bosman A. D., van Dishoeck E. F., 2017, *A&A*, **602**, A105
- Herbst E., Lee H. H., Howe D. A., Millar T. J., 1994, *MNRAS*, **268**, 335
- Hindmarsh A. C., 2019, ODEPACK: Ordinary differential equation solver library (ascl:1905.021)
- Hogerheijde M. R., van der Tak F. F. S., 2000, *A&A*, **362**, 697
- Huebner W. F., Mukherjee J., 2015, *Planet. Space Sci.*, **106**, 11
- Jaber Al-Edhari A., et al., 2017, *A&A*, **597**, A40
- Kahane C., Ceccarelli C., Faure A., Caux E., 2013, *ApJ*, **763**, L38
- Kissel J., et al., 1986, *Nature*, **321**, 280
- Le Roy L., et al., 2015, *A&A*, **583**, A1
- Lichtin D. A., Lin M. C., 1986, *Chemical Physics*, **104**, 325
- Lis D. C., Bockelée-Morvan D., Boissier J., Crovisier J., Biver N., Charnley S. B., 2008, *ApJ*, **675**, 931
- Martins Z., Sephton M. A., 2010, *Amino Acids, Peptides and Proteins in Organic Chemistry: Origins and Synthesis of Amino Acids*, Volume 1, A. B. Hughes (ed.), Wiley, pp 3–42
- McCaffrey V. P., Zellner B. N. E., Waun C. M., Bennett E. R., Earl E. K., 2014, *Origins of Life and Evolution of Biospheres*, **44**, 29
- Mumma M. J., Charnley S. B., 2011, *ARA&A*, **49**, 471
- Mumma M. J., Charnley S., Cordiner M., Villanueva G., Faggi S., Paganini L., Lippi M., DiSanti M. A., 2018, in *AAS/Division for Planetary Sciences Meeting Abstracts #50*, p. 209.02
- Oba Y., Takano Y., Naraoka H., Furukawa Y., Glavin D. P., Dworkin J. P., Tachibana S., 2020, *Nature Communications*, **11**, 6243
- Patel B. H., Percivalle C., Ritson D. J., Duffy C. D., Sutherland J. D., 2015, *Nat. Chem.*, **7**, 301
- Pierazzo E., Chyba C. F., 1999, *Meteoritics and Planetary Science*, **34**, 909
- Poch O., et al., 2020, *Science*, **367**, aaw7462
- Rodgers S. D., Charnley S. B., 2001a, *MNRAS*, **320**, L61
- Rodgers S. D., Charnley S. B., 2001b, *MNRAS*, **323**, 84
- Rodgers S. D., Charnley S. B., 2002, *MNRAS*, **330**, 660
- Rubin M., et al., 2019, *MNRAS*, **489**, 594
- Saladino R., Crestini C., Pino S., Costanzo G., Di Mauro E., 2012, *Physics of Life Reviews*, **9**, 84
- Sims I. R., Queffelec J.-L., Travers D., Rowe B. R., Herbert L. B., Karthäuser J., Smith I. W. M., 1993, *Chemical Physics Letters*, **211**, 461
- Sims I. R., Queffelec J.-L., Defrance A., Rebrion-Rowe C., Travers D., Bocherel P., Rowe B. R., Smith I. W. M., 1994, *Journal of Chemical Physics*, **100**, 4229
- Skouteris D., Vazart F., Ceccarelli C., Balucani N., Puzzarini C., Barone V., 2017, *MNRAS*, **468**, L1
- Talbi D., Smith I. W. M., 2009, *Phys. Chem. Chem. Phys.*, **11**, 8477
- Todd Z. R., Öberg K. I., 2020, *Astrobiology*, **20**, 1109
- Walsh C., Millar T. J., Nomura H., Herbst E., Widicus Weaver S., Aikawa Y., Laas J. C., Vasyunin A. I., 2014, *A&A*, **563**, A33



Wyckoff S., Tegler S., Wehinger P. A., Spinrad H., Belton M. J. S., 1988,  
[ApJ, 325, 927](#)  
Wyckoff S., Tegler S. C., Engel L., 1991, [ApJ, 367, 641](#)

This paper has been typeset from a  $\text{\TeX/L\AA\TeX}$  file prepared by the author.